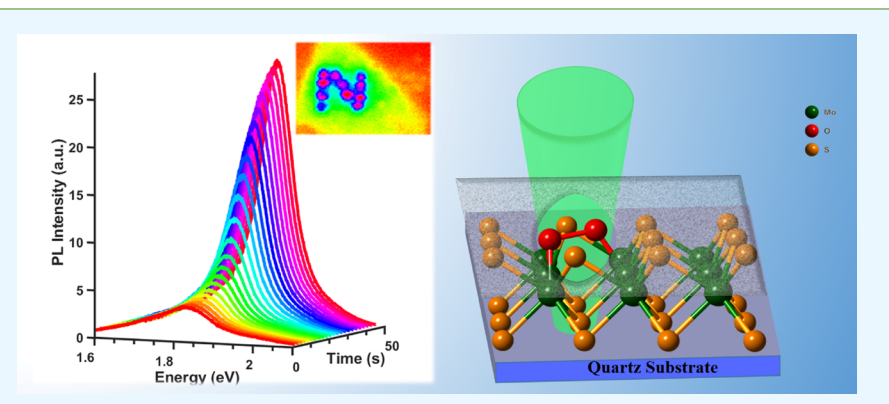


Reversible Photoluminescence Tuning by Defect Passivation via Laser Irradiation on Aged Monolayer MoS₂

Hossein Ardekani, ** Robert Younts, ** Yiling Yu, ** Linyou Cao, ** and Kenan Gundogdu**, ** Linyou Cao, ** and Kenan Gundogdu**, **

Department of Physics and Department of Materials Science and Engineering, North Carolina State University, Raleigh, North Carolina 27695, United States

Supporting Information



ABSTRACT: Atomically thin (1L)-MoS₂ emerged as a direct band gap semiconductor with potential optical applications. The photoluminescence (PL) of 1L-MoS2 degrades due to aging-related defect formation. The passivation of these defects leads to substantial improvement in optical properties. Here, we report the enhancement of PL on aged 1L-MoS₂ by laser treatment. Using photoluminescence and Raman spectroscopy in a gas-controlled environment, we show that the enhancement is associated with efficient adsorption of oxygen on existing sulfur vacancies preceded by removal of adsorbates from the sample's surface. Oxygen adsorption depletes negative charges, resulting in suppression of trions and improved neutral exciton recombination. The result is a 6- to 8-fold increase in PL emission. The laser treatment in this work does not cause any measurable damage to the sample as verified by Raman spectroscopy, which is important for practical applications. Surprisingly, the observed PL enhancement is reversible by both vacuum and ultrafast femtosecond excitation. While the former approach allows switching a designed micropattern on the sample ON and OFF, the latter provides a controllable mean for accurate PL tuning, which is highly desirable for optoelectronic and gas sensing applications.

KEYWORDS: MoS2, photoluminescence, Raman, reversible defect passivation, exciton, oxygen, laser annealing

■ INTRODUCTION

Atomically thin transition-metal dichalcogenides (TMDs) exhibit unique optical and electronic properties due to their 2D electronic structure. 1-4 Specifically, monolayer MoS2 and WS₂ are direct gap semiconductors, and therefore, their photoluminescence (PL) is stronger compared to indirect gap multilayer materials.^{5,6} However, due to both intrinsic defects and aging-related degradation⁸ in these materials, PL efficiency reduces considerably. A significant amount of research is focused on characterization of the defects^{9,10} and improving the optical properties by defect passivation in 2D materials. 11-13 The chalcogenide (S and Se) vacancies are the primary sources of defects. 14 These vacancies facilitate interaction of 2D materials with ambient reactants and promote oxidation. Several different methods have been utilized to control the oxidation state of defects. These include superacid treatment, 15,16 electrical gating, 17 and chemical doping. 18-20 These treatments remove the surface adsorbates

and passivate defects, which in turn lead to high PL quantum efficiency.

Existence of defects also increases the sensitivity of 2D materials to ambient conditions, as they interact with molecular and atomic adsorbates. 21 Specifically, ambient oxygen is capable of forming strong bonds at defect sites. 12 Numerous experimental studies have been performed to investigate the impact of oxygen adsorption on optical and electronic properties of monolayer (1L) TMDs.²²⁻²⁵ Whether the interaction of oxygen molecules with defect sites enhances the optical properties 12 or degrades the sample permanently 26 is ambiguous. In this communication, we report a highly controllable and reversible enhancement of the PL of aged 1L-MoS₂, using laser irradiation. Our results show that sufficient laser heating in the presence of oxygen removes surface

Received: June 18, 2019 Accepted: September 10, 2019 Published: September 10, 2019 contaminants on the aged sample, exposing existing sulfur vacancies²⁷ to ambient. Subsequent adsorption of oxygen at defect sites depletes excess negative charges in the material, suppresses trion²⁸ formation, and increases neutral exciton recombination efficiency. We demonstrate that such oxygen adsorption is a reversible process. Both introduction of vacuum and ultrashort pulse excitation are capable of removing the oxygen from the defect sites. While the former method may be utilized to hide a micropattern carved on sample's surface temporarily, the latter approach leads to fast modulation of optical and electronic properties of monolayer MoS₂, which is highly demanded in optoelectronic applications such as gas sensing.

RESULTS

1L-MoS $_2$ was synthesized, transferred on quartz substrates (see Methods for details), and kept in room temperature and under an ambient condition undergoing normal aging. 6–18 monthaged samples were used for all PL and Raman measurements. All optical measurements were performed on samples located in a chamber with gas control. To treat the samples, a diodepumped solid-state laser beam at 532 nm was focused at a 1.1 μ m spot on monolayer MoS $_2$ using a 50× objective. During the treatment process, the chamber was filled with oxygen gas at 1.5 atm. Figure 1a shows the PL spectrum evolving over a span of 30 s during laser treatment. A fixed 22 mW laser beam (1.8 MW/cm 2) is exciting the sample. The incident light plays a double role, as a mean for laser treatment and as an excitation source for PL measurements. It can be seen that the intensity rises almost immediately once the laser is incident on the

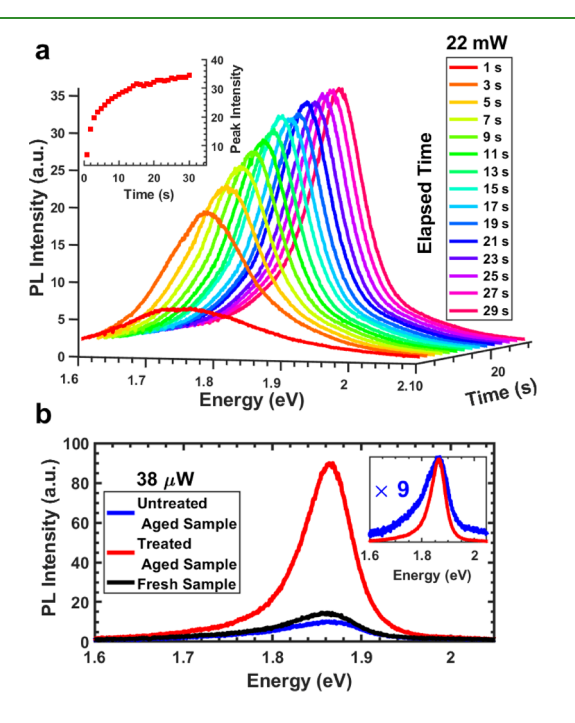


Figure 1. (a) Laser treatment of the sample: Time evolution of photoluminescence spectra on aged $1L\text{-MoS}_2$ at constant photoexcitation using 532 nm CW laser with a power of 22 mW. The inset shows how the peak intensity changes while laser treatment taking place. (b)Comparison of fresh andaged samples PL spectra before and after laser treatment. These excitation power is 38 μ W.. The inset shows normalized PL of aged sample before and after the treatment, depicting the PL spectral shape narrowed due to laser treatment.

sample. As shown in the inset of Figure 1a, after a fast rise, the PL evolution ceases and gradually reaches saturation. Figure S1 (see the Supporting Information) demonstrates that while the laser treatment is taking place, the PL spectrum narrows and the peak blue shifts. To confirm the role of oxygen in the process, we performed gas-controlled experiments under vacuum, Ar, N₂, and ambient air conditions. Figure S2 shows that laser treatment does not occur in Ar, N₂ or vacuum but sets off once air is released in the experimental chamber. The slower PL evolution in air demonstrated in Figure S3 (see the Supporting Information) compared to the same process in pure oxygen (Figure 1a) confirms the dominant role of oxygen in the observed phenomenon.

We then analyzed the spectral changes of PL to infer modifications incurred to the material. Figure 1b shows comparison of the PL spectrum on fresh and aged samples before and after the treatment. Excitation power of $38~\mu W~(3.1~kW/cm^2)$ is chosen low enough such that local heating effects are safely neglected. Compared to a fresh sample, aged 1L-MoS₂ shows almost 50% weaker PL intensity. The laser treatment, however, enhances the PL by factor of 9. Comparison of the normalized PL before and after laser treatment shown in Figure 1b inset signifies the reduction in spectral width after laser treatment. Such a change is direct indication of defect passivation. As a result, the trion density reduces and the emission is dominated by exciton recombination. 13

To quantify the contribution of trion and exciton recombination to the PL, we fit A and B exciton 29 PL features to a convolution of Gaussian and Lorentzian lineshape functions (Voigt). For the trion (A $^-$) feature, we used a Gaussian convolved with an exponential decay on the lower energy side. 30 Figure 2a,b shows the fit curves for the PL

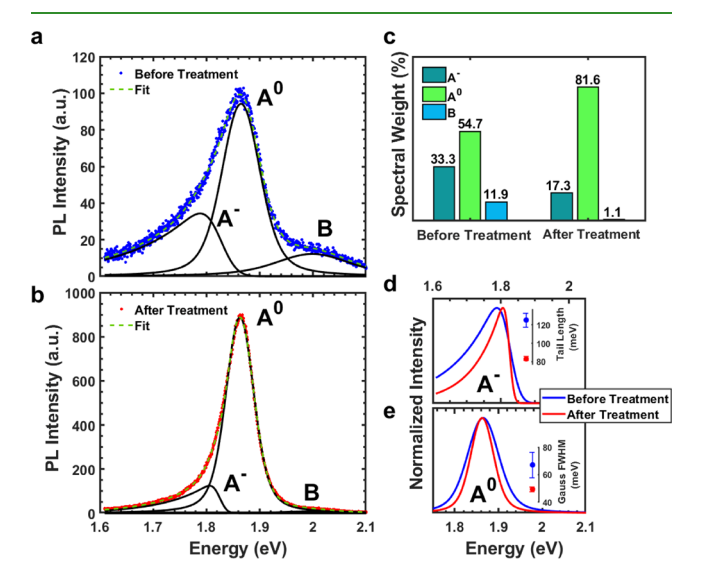


Figure 2. Spectral analysis performed on PL measured with 38 μ W excitation power (a) before and (b) after laser treatment. Each spectrum comprises of three components: A^- , A^0 , and B peaks. Convolution of Gaussian and Lorentzian (Voigt function) is used to fit A^0 and B exciton peaks and exponentially modified Gaussian on its low energy tail used for the A^- peak. (c) Comparison of the spectral weight of A^0 , A^- , and B peaks before and after treatment. Normalized fit curves for (d) A^- and (e) A^0 peaks before and after treatment. The insets compare the low energy exponential tail length and Gaussian FWHM.

ACS Applied Materials & Interfaces

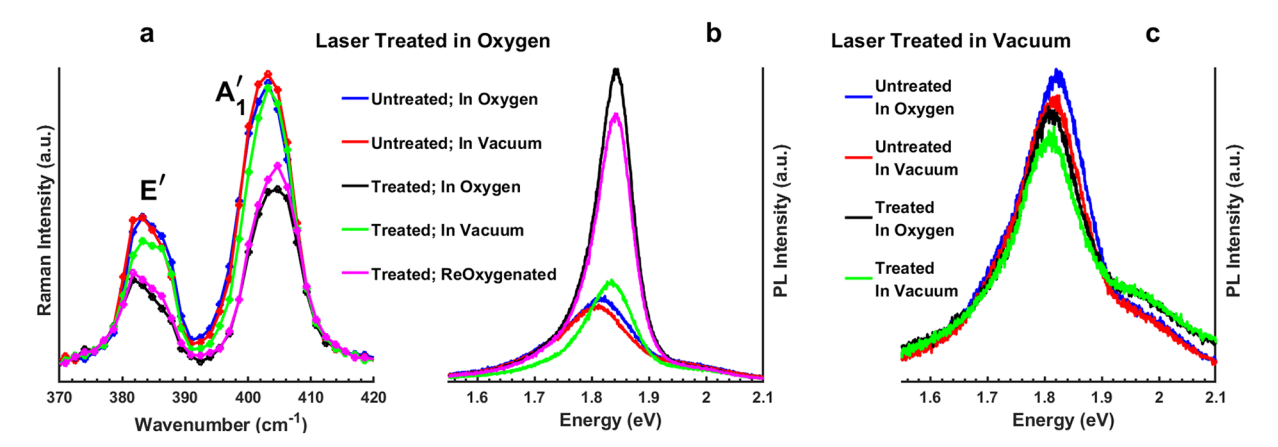


Figure 3. Comparison of (a) Raman and (b) PL spectra in various ambient conditions before and after the laser treatment performed in oxygen ambient. (c) PL spectrum in various ambient conditions before and after laser treatment performed in vacuum. In all panels, blue and red curves correspond to spectra obtained before laser treatment while the sample is in oxygen and vacuum, respectively. Black and green curves are related to the spectra after treatment was performed keeping the sample in oxygen and vacuum, respectively. The pink curve in panels (a) and (b) corresponds to releasing the oxygen back into the chamber following the vacuuming performed after laser treatment. The measurements were performed consecutively starting from the untreated sample in oxygen and ending with reoxygenated, treated sample. Treatment was performed only once before collecting black curve data.

spectra before and after treatment, respectively. Both spectra show the B exciton at 2.00 eV, neutral A exciton peak (A⁰) at 1.86 eV, and A⁻ peak at 1.82 eV. The spectral weight of each feature is calculated by dividing the integrated PL intensity of fit curves by the integrated total PL intensity. As can be seen in Figure 2c, 33.3% contribution of the A⁻ is almost reduced to 17.3% after laser treatment. On the other hand, A⁰ recombination became the dominant radiative mechanism after laser treatment, contributing to more than 80% of the PL spectral shape.

The suppression of trions has been previously reported and explained based on oxygen adsorption occurring on defect sites. 12 Sulfur vacancies create excess free electrons. Oxygen molecules depletes these electrons, hence p-doping the material. 18 More detailed spectral analysis of neutral exciton and trion line shapes further reveals the p-doping nature of the treatment process. Figure 2d,e shows the normalized fit curves before and after treatment for A and A⁰, respectively. The low-energy exponential tail in the A⁻ line shape originates from the recombination of the nonzero momentum trions and is an indicator of their thermal distribution,³⁰ while the full width at half-maximum (FWHM) of the A⁰ Gaussian is directly related to the local temperature and thermal distribution of the neutral excitons. As shown in the inset of Figure 2d, the exponential tail length of trions is decreased after the laser treatment, demonstrating lower local temperature generated by incident laser excitation. This justifies less trion formation since their recombination tends to locally heat the sample via Auger processes. Lower local temperature is also reflected in the reduced Gaussian FWHM of the A⁰, as can be observed in the inset of Figure 2e. Both parameters verify the p-doping occurred and suppression of trions as a result of laser treatment.

Previous studies have shown that p-doping of $1L\text{-MoS}_2$ affects its Raman vibrational modes. Figure 3a shows the Raman spectra for E' and A'₁ modes before and after treatment in various ambient conditions. As expected, before laser treatment, the change in the ambient gas does not modify the Raman spectrum (blue versus red curve in Figure 3a). Laser treatment blue shifts the A'₁ mode as long as the sample is kept

in oxygen (black curve in Figure 3a); meanwhile, the E' mode red shifts (see Figure S4a for details, Supporting Information). The stiffening of the A'₁ mode observed in the Raman spectrum after laser treatment and in the presence of oxygen is in full agreement with the p-doping effect³² expected from oxygen adsorption. On the other hand, the change in the E' mode reflects the variation in the tensile strain among crystalline atoms.³³ The change in strain is expected to occur if a sulfur vacancy is created in a spot or inversely, an existing sulfur vacancy is filled with adsorption of a compensating atom. 10 It is also important to note that after laser treatment, the peak intensities for both A'₁ and E' are reduced. To confirm the intensity reduction is not due to laser induced damages,³⁴ we vacuumed the chamber and repeated the Raman measurement. The Raman spectrum reaches to the initial value (green curve in Figure 3a) upon vacuuming, clearly verifying no measurable damage occurred to the sample. The change in the Raman spectra is reversible, that is, introduction of oxygen back into the chamber reverts both modes to their previous intensity levels and spectral positions (see Figure S4, Supporting Information).

Similar to the Raman spectrum, the PL intensity is very sensitive to the ambient gas after performing the laser treatment. Figure 3b shows that after the sample is laser treated in oxygen ambient, PL increases (black curve), subsequent vacuuming reduces the PL (green), and reintroducing the oxygen increases the PL (pink). This reversible change in PL and Raman spectra by mere introduction of vacuum illustrates that p-doping of the sample is due to physisorbed oxygen molecules, which can be removed from the surface relatively easy.

DISCUSSION

The presented results clearly show laser treatment of monolayer MoS_2 in oxygen ambient conditions, which reduces free charges and trion recombination and therefore improves PL efficiency. One potential explanation for these observed phenomena is introduction of more sulfur vacancies to the sample via laser irradiation, hence increasing the chance of oxygen adsorption. It has been previously reported that defect

density on monolayer MoS_2 can be increased by various means including laser irradiation. ^{35,36} However, such processes take place in a considerably longer time scale than what we observed in our experiments. On the other hand, our results could not be reproduced on fresh samples (Figure S5), confirming the underlying mechanism to be more than only creating extra defect sites on the sample.

Figure 3c shows the laser treatment of the sample in vacuum. Here, the PL does not improve, even if the oxygen is introduced after treatment. This suggests that laser irradiation alone is not only removing the contaminants from the 2D material³⁷ but instead there is a chemical reaction taking place. Earlier works showed that oxygen interacts with defects via both chemisorption and physisorption. 38-40 Chemisorption requires splitting of oxygen molecules into atoms and forming strong Mo-O bonds in the lattice. On the other hand, physisorption forms by weak van der Waals interaction between O2 molecules and sulfur vacancies. Computational studies suggest that oxygen dissociation at the MoS2 defect sites requires overcoming a potential barrier around 1 eV. 40-42 According to kinetic theory, this energy can be provided at 450 K.⁴³ In our experiments, local heating due to laser excitation can facilitate dissociation of O2. We used Raman spectroscopy to estimate the local temperature under 22 mW photoexcitation (see section 4, Supporting Information). Our temperature evaluation reveals that the local temperature rises up to 440 K, which is in perfect agreement with previously reported values required to overcome oxygen dissociation barrier at defect sites.4

We note that the formation of stable chemisorbed oxygen bonds is in direct contrast of reversibility of PL under vacuum. Furthermore, the tensile strain due to formation of Mo-O bonds, which can be observed as the red shift of the E' mode in Raman spectra (black curve in Figure 3a), should not change under vacuum, but it does. Therefore, oxygen chemisorption cannot fully explain our experimental results, although it might take place as a secondary process. Previous studies show that chemisorption of oxygen occurs much slower than oxygen physisorption.²⁴ We conclude then that during the laser treatment, oxygen catalyzes the removal of other adsorbates from the surface. This exposes the already existing sulfur vacancies to oxygen molecules as schematically demonstrated in Figure 4a. Such a cleaning process prepares defect sites for efficient O2 physisorption while oxygen chemisorption may occur at a lower rate (see section 5, Supporting Information).

Since removal of oxygen has a dramatic effect on PL, it can be used to switch or tune the optical properties of monolayer MoS₂. Enhancing the PL on 1L-TMDs by laser irradiation is a promising tool to generate desired micropatterns on the surface of the sample. 44,45 However, controlling the intensity of the emitted light does not seem to be possible in previously reported methods, and created patterns stay bright compared to the adjacent area. Figure 4b shows the PL image (see Methods for details) of a 1L-MoS₂ flake, where the letter "N" is generated using the laser treatment as described earlier. As illustrated in Figure 4c, subsequent vacuuming makes the pattern almost invisible. However, the treated spots stay highly reactive, and as shown in Figure 4d, reintroducing oxygen into the chamber brightens up the treated spots. Fine-tuning the PL, on the other hand, is possible via removing oxygen molecules from defects temporarily by applying ultrashort femtosecond (fs) laser pulses. Figure 5 shows the effect of fs

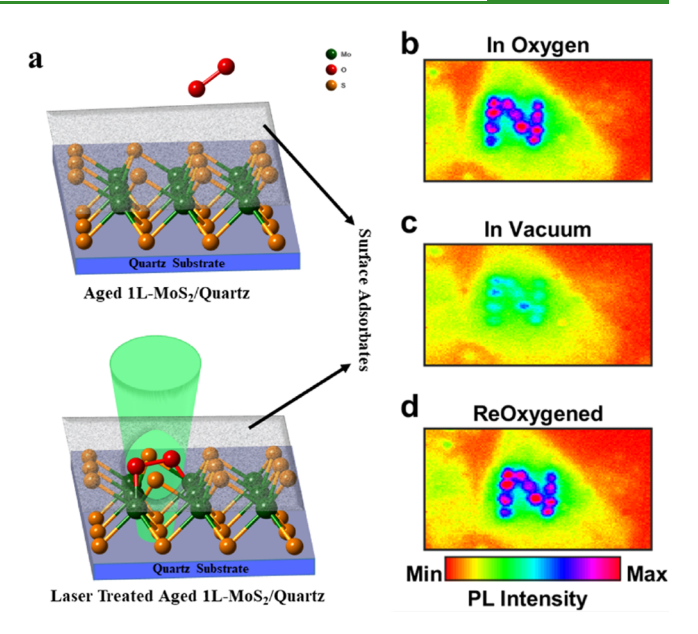


Figure 4. (a) Schematic demonstration of laser treatment process on aged 1L-MoS₂. On the top, there is a view of the aged sample with a sulfur vacancy. At the bottom, surface cleaning + oxygen physisorption on the defect site facilitated by laser treatment is depicted. The PL image of a monolayer flake is shown where the letter "N" is produced using laser treatment (b) in the presence of oxygen, (c) in vacuum, and (d) after reintroducing the oxygen.

excitation on the PL spectrum of the laser-treated sample. The PL is measured with 38 μ W of continuous wave (CW) excitation. To control the PL intensity, we excite the same spot with fs pulses (see Methods for details) at different excitation fluences. The narrow and enhanced PL of the treated sample (red curves) can be tuned (black curves) down to the PL of the untreated sample (blue curves). Once the fs excitation is ceased, the PL rises again (green curves). The recovery time of the PL depends on fs excitation fluence used. At higher fluences, it takes longer for the PL to reach back to the treated sample PL intensities (see section 6 for details, Supporting Information).

CONCLUSIONS

In this letter, we investigated the laser treatment process, which helps recovering and further enhancing the PL on the aged 1L-MoS₂. We observe that irradiating the sample with the CW laser beam cleans the 2D material surface and exposes already existing sulfur vacancies to oxygen molecules. This process facilitates physisorption and eventually chemisorption of oxygen at defect sites, giving rise to depletion of negative charges, hence suppressing trion formation and enhancing neutral exciton recombination. The p-doping due to adsorption of oxygen molecules is confirmed by our PL spectral analysis and Raman spectroscopy measurements. The reversibility of the PL enhancement in vacuum enables turning ON and OFF of a designed pattern on the sample's surface. Furthermore, we showed that introducing fs laser pulses to the treated sample promotes fast, reversible, and broad range modulation of the PL. Other than accurate and reversible modulation of the PL, the laser treatment of aged 1L-MoS₂ provides high sensitivity to oxygen adsorption. Room-temperature operation, along with high responsivity, and fast recovery time are remarkable features achieved by introducing ultrafast

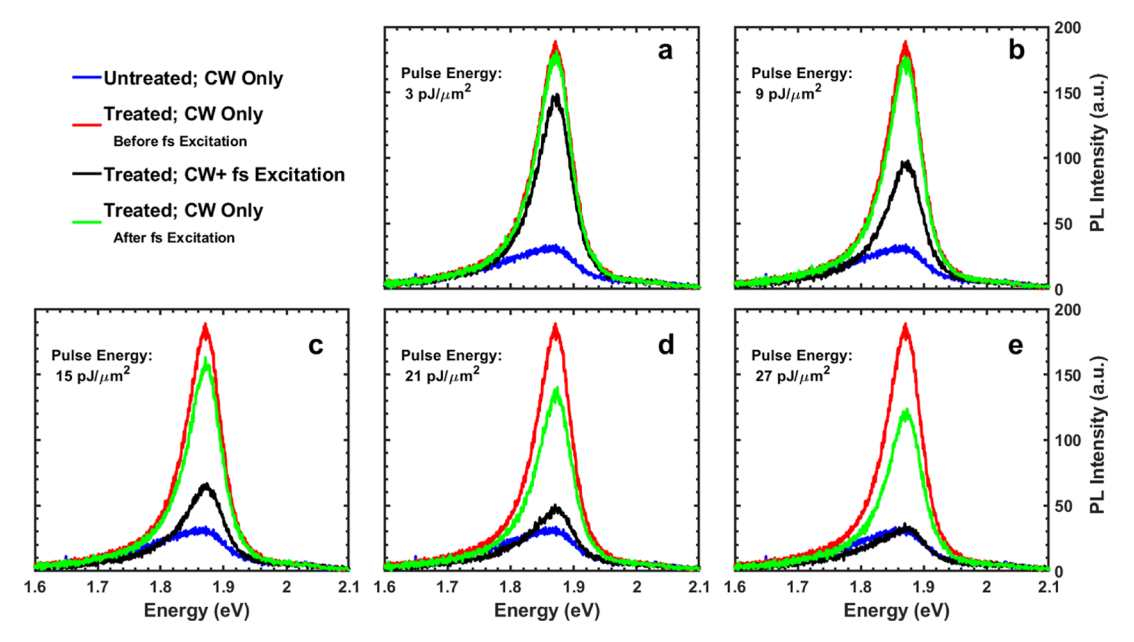


Figure 5. Reversible PL tuning by applying fs laser pulses on laser treated 1L-MoS₂. In all panels, blue and red curves are the PL before and 10 s after treatment, respectively, with CW excitation only. Black curves correspond to PL measured with simultaneous CW and fs excitation at (a) 3, (b) 6, (c) 9, (d) 12, and (e) 15 pJ/um² pulse energy. Green curves are PL collected by CW only excitation after 10 s of blocking fs pulses. 38 µW power used for all CW excitation. Treatment was performed only once before collecting red curve data. The measurements were performed consecutively starting from the blue curve and ending with the green curve.

laser pulses to the treated sample, making it a promising approach for gas sensing applications. 46-49

METHODS

Sample Preparation. Two-dimensional (2D) layer MoS2 was grown on a sapphire substrate by chemical vapor deposition. Monolayer MoS2 was manually transferred onto the quartz substrate suing a surface energy-assisted method. The two samples under study (12 and 18 month aged) were kept at room temperature in an ambient condition.

PL Measurements. For CW only excitation, a diode-pumped solid state laser (Verdi, Coherent) beam at 532 nm was used along with variable neutral density filters to adjust the laser power. A glass thickness-compensated ultralong working distance 50× objective lens (NA = 0.5) was used to focus the laser on the sample. The power was measured before the objective using a power meter (Thorlabs S121C). The PL was collected by the same objective and passed through a dielectric 550 nm long-pass filter to block the fundamental 532 nm line. The light was then focused onto the slit of the spectrometer using a 2× lens. The PL was spectrally resolved by a spectrometer (Acton SP2300) with a 300 grooves mm⁻¹ grating and imaged by a deep cooled CCD camera (PIXIS).

For fs + CW excitation experiments, the CW 532 nm laser light described above was coupled to fs pulses using a 50–50% beam splitter. Fs laser pulses were generated by a Ti–sapphire ultrafast laser system (Mira 900, Coherent + Rega 9000, Coherent). The amplified fs pulses were sent to an optical parametric amplifier (OPA 9400, Coherent), and 532 nm pulses with 100 fs pulse width at 250 kHz output from the OPA were selected. The choice of 532 nm wavelength from the OPA was merely to match in focus after the objective lens for both CW and fs beams, since different wavelengths have slightly different focal points.

To take PL images, CW 532 nm laser light was focused on the sample at 45° angle with respect to normal using a 75 mm lens. This created an almost uniformly illuminated area around 500 um². Power (700 μ W) was chosen to avoid any disruption on the laser-treated spots. The PL was then collected normal to the sample using the same geometry explained for CW only excitations above.

Raman Measurements. The same setup was used as in PL measurements, except the long-pass filter being replaced by a 533 nm notch filter with 17 nm FWHM (Thorlabs NF533-17), which allowed the acquisition of both Stokes and anti-Stokes scattered light simultaneously and switching the grating to a 1200 grooves mm⁻¹ one.

ASSOCIATED CONTENT

S Supporting Information

The Supporting Information is available free of charge on the ACS Publications website at DOI: 10.1021/acsami.9b10688.

PL treatment in various ambient conditions, Raman spectral analysis, temperature estimation, aging and adsorption mechanism, and further PL tuning (PDF)

AUTHOR INFORMATION

Corresponding Author

*E-mail: kgundog@ncsu.edu.

ORCID ©

Hossein Ardekani: 0000-0002-1274-8978

Yiling Yu: 0000-0001-7180-1137 Linyou Cao: 0000-0002-7834-8336 Kenan Gundogdu: 0000-0001-7149-5766

Notes

The authors declare no competing financial interest.

ACKNOWLEDGMENTS

This work was funded by NSF DMR-1709934. The authors acknowledge the discussions and insights from Dr. Ale Bataller.

REFERENCES

(1) Wang, Q. H.; Kalantar-Zadeh, K.; Kis, A.; Coleman, J. N.; Strano, M. S. Electronics and Optoelectronics of Two-Dimensional Transition Metal Dichalcogenides. *Nat. Nanotechnol.* **2012**, *7*, 699–712.

- (2) Bataller, A. W.; Younts, R. A.; Rustagi, A.; Yu, Y.; Ardekani, H.; Kemper, A.; Cao, L.; Gundogdu, K Dense Electron—Hole Plasma Formation and Ultralong Charge Lifetime in Monolayer MoS₂ via Material Tuning. *Nano Lett.* **2019**, 1104.
- (3) Lopez-Sanchez, O.; Lembke, D.; Kayci, M.; Radenovic, A.; Kis, A. Ultrasensitive Photodetectors Based on Monolayer MoS₂. *Nat. Nanotechnol.* **2013**, *8*, 497–501.
- (4) Pospischil, A.; Furchi, M. M.; Mueller, T. Solar-Energy Conversion and Light Emission in an Atomic Monolayer p-n Diode. *Nat. Nanotechnol.* **2014**, *9*, 257–261.
- (5) Tongay, S.; Zhou, J.; Ataca, C.; Lo, K.; Matthews, T. S.; Li, J.; Grossman, J. C.; Wu, J. Thermally Driven Crossover from Indirect toward Direct Bandgap in 2D Semiconductors: MoSe₂ versus MoS₂. *Nano Lett.* **2012**, *12*, 5576–5580.
- (6) Splendiani, A.; Sun, L.; Zhang, Y.; Li, T.; Kim, J.; Chim, C. Y.; Galli, G.; Wang, F. Emerging Photoluminescence in Monolayer MoS₂. *Nano Lett.* **2010**, *10*, 1271–1275.
- (7) Zhou, W.; Zou, X.; Najmaei, S.; Liu, Z.; Shi, Y.; Kong, J.; Lou, J.; Ajayan, P. M.; Yakobson, B. I.; Idrobo, J.-C. Intrinsic Structural Defects in Monolayer Molybdenum Disulfide. *Nano Lett.* **2013**, 2615.
- (8) Pető, J.; Ollár, T.; Vancsó, P.; Popov, Z. I.; Magda, G. Z.; Dobrik, G.; Hwang, C.; Sorokin, P. B.; Tapasztó, L. Spontaneous Doping of the Basal Plane of MoS₂ Single Layers through Oxygen Substitution under Ambient Conditions. *Nat. Chem.* **2018**, *10*, 1246–1251.
- (9) Lin, Z.; Carvalho, B. R.; Kahn, E.; Lv, R.; Rao, R.; Terrones, H.; Pimenta, M. A.; Terrones, M. Defect Engineering of Two-Dimensional Transition Metal Dichalcogenides. 2D Mater 2016, 3, No. 022002.
- (10) Zhao, B.; Shang, C.; Qi, N.; Chen, Z. Y.; Chen, Z. Q. Stability of Defects in Monolayer MoS₂ and Their Interaction with O₂ Molecule: A First-Principles Study. *Appl. Surf. Sci.* **2017**, *412*, 385–393.
- (11) Shu, H.; Li, Y.; Niu, X.; Wang, J. Greatly Enhanced Optical Absorption of a Defective MoS₂ Monolayer through Oxygen Passivation. ACS Appl. Mater. Interfaces 2016, 8, 13150–13156.
- (12) Nan, H.; Wang, Z.; Wang, W.; Liang, Z.; Lu, Y.; Chen, Q.; He, D.; Tan, P.; Miao, F.; Wang, X.; et al. Strong Photoluminescence Enhancement of MoS₂ through Defect Engineering and Oxygen Bonding. ACS Nano 2014, 8, 5738–5745.
- (13) Tongay, S.; Zhou, J.; Ataca, C.; Liu, J.; Kang, J. S.; Matthews, T. S.; You, L.; Li, J.; Grossman, J. C.; Wu, J. Broad-Range Modulation of Light Emission in Two-Dimensional Semiconductors by Molecular Physisorption Gating. *Nano Lett.* **2013**, *13*, 2831–2836.
- (14) Hong, J.; Hu, Z.; Probert, M.; Li, K.; Lv, D.; Yang, X.; Gu, L.; Mao, N.; Feng, Q.; Xie, L.; Zhang, J.; Wu, D.; Zhang, Z.; Jin, C.; Ji, W.; Zhang, X.; Yuan, J.; Zhang, Z. Exploring Atomic Defects in Molybdenum Disulphide Monolayers. *Nat. Commun.* **2015**, *6*, 6293.
- (15) Amani, M.; Lien, D.-H.; Kiriya, D.; Xiao, J.; Azcatl, A.; Noh, J.; Madhvapathy, S. R.; Addou, R.; KC, S.; Dubey, M.; et al. Near-Unity Photoluminescence Quantum Yield in MoS2. *Science* **2015**, *350*, 1065–1068.
- (16) Amani, M.; Burke, R. A.; Ji, X.; Zhao, P.; Lien, D.-H.; Taheri, P.; Ahn, G. H.; Kirya, D.; Ager, J. W., III; Yablonovitch, E.; et al. High Luminescence Efficiency in MoS ₂ Grown by Chemical Vapor Deposition. *ACS Nano* **2016**, *10*, 6535–6541.
- (17) Atallah, T. L.; Wang, J.; Bosch, M.; Seo, D.; Burke, R. A.; Moneer, O.; Zhu, J.; Theibault, M.; Brus, L. E.; Hone, J.; et al. Electrostatic Screening of Charged Defects in Monolayer MoS2. *J. Phys. Chem. Lett.* **2017**, *8*, 2148–2152.
- (18) Mouri, S.; Miyauchi, Y.; Matsuda, K. Tunable Photoluminescence of Monolayer MoS₂ via Chemical Doping. *Nano Lett.* **2013**, *13*, 5944–5948.
- (19) Zhou, C.; Zhao, Y.; Raju, S.; Wang, Y.; Lin, Z.; Chan, M.; Chai, Y. Carrier Type Control of WSe₂ Field-Effect Transistors by Thickness Modulation and MoO₃ Layer Doping. *Adv. Funct. Mater.* **2016**, 4223–4230.

- (20) Xu, K.; Wang, Y.; Zhao, Y.; Chai, Y. Modulation Doping of Transition Metal Dichalcogenide/Oxide Heterostructures. *J. Mater. Chem. C* **2017**, *5*, 376–381.
- (21) Martincová, J.; Otyepka, M.; Lazar, P. Is Single Layer MoS₂ Stable in the Air? *Chem. Eur. J.* **2017**, *23*, 13233–13239.
- (22) Lee, Y.; Ghimire, G.; Roy, S.; Kim, Y.; Seo, C.; Sood, A. K.; Jang, J. I.; Kim, J. Impeding Exciton-Exciton Annihilation in Monolayer WS₂ by Laser Irradiation. *ACS Photonics* **2018**, *5*, 2904–2911.
- (23) Wei, X.; Yu, Z.; Hu, F.; Cheng, Y.; Yu, L.; Wang, X.; Xiao, M.; Wang, J.; Wang, X.; Shi, Y. Mo-O Bond Doping and Related-Defect Assisted Enhancement of Photoluminescence in Monolayer MoS₂. *AIP Adv.* **2014**, *4*, 123004.
- (24) Qi, L.; Wang, Y.; Shen, L.; Wu, Y. Chemisorption-inducedndoping of MoS₂ by Oxygen. *Appl. Phys. Lett.* **2016**, *108*, 063103.
- (25) Chow, W. L.; Luo, X.; Quek, S. Q.; Tay, B. K. Evolution of Raman Scattering and Electronic Structure of Ultrathin Molybdenum Disulfide by Oxygen Chemisorption. *Adv. Electron. Mater.* **2015**, *1*, 1400037.
- (26) Kang, N.; Paudel, H. P.; Leuenberger, M. N.; Tetard, L.; Khondaker, S. I. Photoluminescence Quenching in Single-Layer MoS₂ via Oxygen Plasma Treatment. *J. Phys. Chem. C* **2014**, *118*, 21258–21263.
- (27) Gao, J.; Li, B.; Tan, J.; Chow, P.; Lu, T.-M.; Koratkar, N. Aging of Transition Metal Dichalcogenide Monolayers. *ACS Nano* **2016**, *10*, 2628.
- (28) Mak, K. F.; He, K.; Lee, C.; Lee, G. H.; Hone, J.; Heinz, T. F.; Shan, J. Tightly Bound Trions in Monolayer MoS 2. *Nat. Mater.* **2013**, *12*, 207–211.
- (29) Qiu, D. Y.; da Jornada, F. H.; Louie, S. G. Optical Spectrum of MoS2: Many-Body Effects and Diversity of Exciton States. *Phys. Rev. Lett.* **2013**, 216805.
- (30) Christopher, J. W.; Goldberg, B. B.; Swan, A. K Long Tailed Trions in Monolayer MoS_2 : Temperature Dependent Asymmetry and Resulting Red-Shift of Trion Photoluminescence Spectra. *Sci. Rep.* **2017**, *7*, 14062.
- (31) Rao, R.; Islam, A. E.; Campbell, P. M.; Vogel, E. M.; Maruyama, B In situ thermal Oxidation Kinetics in Few Layer MoS₂. 2D Mater. **2017**, *4*, 025058.
- (32) Chakraborty, B.; Bera, A.; Muthu, D. V. S.; Bhowmick, S.; Waghmare, U. V.; Sood, A. K. Symmetry-Dependent Phonon Renormalization in Monolayer MoS₂ transistor. *Phys. Rev. B* **2012**, 85, 161403.
- (33) Lloyd, D.; Liu, X.; Christopher, J. W.; Cantley, L.; Wadehra, A.; Kim, B. L.; Goldberg, B. B.; Swan, A. K.; Bunch, J. S. Band Gap Engineering with Ultralarge Biaxial Strains in Suspended Monolayer MoS2. *Nano Lett.* **2016**, *16*, 5836–5841.
- (34) Paradisanos, I.; Kymakis, E.; Fotakis, C.; Kioseoglou, G.; Stratakis, E. Intense Femtosecond Photoexcitation of Bulk and Monolayer MoS2. *Appl. Phys. Lett.* **2014**, *105*, 041108.
- (35) Bera, A.; Muthu, D. V. S.; Sood, A. K. Enhanced Raman and Photoluminescence Response in Monolayer MoS₂ due to Laser Healing of Defects. *J. Raman Spectrosc.* **2018**, *49*, 100–105.
- (36) Oh, H. M.; Han, G. H.; Kim, H.; Bae, J. J.; Jeong, M. S.; Lee, Y. H. Photochemical Reaction in Monolayer MoS₂ via Correlated Photoluminescence, Raman Spectroscopy, and Atomic Force Microscopy. *ACS Nano* **2016**, *10*, 5230–5236.
- (37) He, Z.; Wang, X.; Xu, W.; Zhou, Y.; Sheng, Y.; Rong, Y.; Smith, J. M.; Warner, J. H. Revealing Defect-State Photoluminescence in Monolayer WS2by Cryogenic Laser Processing. *ACS Nano* **2016**, *10*, 5847–5855.
- (38) Liu, H.; Han, N.; Zhao, J. Atomistic Insight into the Oxidation of Monolayer Transition Metal Dichalcogenides: From Structures to Electronic Properties. *RSC Adv.* **2015**, *5*, 17572–17581.
- (39) Lu, H.; Kummel, A.; Robertson, J. Passivating the Sulfur Vacancy in Monolayer MoS2. *APL Mater.* **2018**, *6*, 066104.
- (40) Kc, S.; Longo, R. C.; Wallace, R. M.; Cho, K. Surface Oxidation Energetics and Kinetics on MoS2monolayer. *J. Appl. Phys.* **2015**, *117*, 135301.

- (41) Spychalski, W. L.; Pisarek, M.; Szoszkiewicz, R. Microscale Insight into Oxidation of Single MoS₂ Crystals in Air. *J. Phys. Chem. C* **2017**, *121*, 26027–26033.
- (42) González, C.; Biel, B.; Dappe, Y. J. Adsorption of Small Inorganic Molecules on a Defective MoS2 monolayer. *Phys. Chem. Chem. Phys.* **2017**, *19*, 9485–9499.
- (43) Supporting Information for Nan, H.; Wang, Z.; Wang, W.; Liang, Z.; Lu, Y.; Chen, Q.; He, D.; Tan, P.; Miao, F.; Wang, X.; Wang, J.; Ni, Z. Strong Photoluminescence Enhancement of MoS₂ through Defect Engineering and Oxygen Bonding. *ACS Nano* **2014**, 8, 5738–5745.
- (44) Sivaram, S. V.; Hanbicki, A. T.; Rosenberger, M. R.; Jernigan, G. G.; Chuang, H.-J.; McCreary, K. M.; Jonker, B. T Spatially Selective Enhancement of Photoluminescence in MoS₂ by Exciton-Mediated Adsorption and Defect Passivation. ACS Appl. Mater. Interfaces 2019, 16147.
- (4\$\tilde{S}\$) Lu, J.; Lu, J. H.; Liu, H.; Liu, B.; Chan, K. X.; Lin, J.; Chen, W.; Loh, K. P.; Sow, C. H. Improved Photoelectrical Properties of MoS₂ Films after Laser Micromachining. *ACS Nano* **2014**, *8*, 6334–6343.
- (46) Zeng, S.; Hu, S.; Xia, J.; Anderson, T.; Dinh, X.-Q.; Meng, X.-M.; Coquet, P.; Yong, K.-T. Graphene—MoS₂ Hybrid Nanostructures Enhanced Surface Plasmon Resonance Biosensors. *Sens. Actuators, B.* **2015**, 207, 801–810.
- (47) Donarelli, M.; Ottaviano, L. 2D Materials for Gas Sensing Applications: A Review on Graphene Oxide, MoS₂, WS₂ and Phosphorene. *Sensors* **2018**, *18*, 3638.
- (48) Li, H.; Yin, Z.; He, Q.; Li, H.; Huang, X.; Lu, G.; Fam, D. W. H.; Tok, A. I. Y.; Zhang, Q.; Zhang, H. Fabrication of Single- and Multilayer MoS 2 Film-Based Field-Effect Transistors for Sensing NO at Room Temperature. *Small* **2012**, 63–67.
- (49) Arafat, M. M.; Dinan, B.; Akbar, S. A.; Haseeb, A. S. M. A. Gas Sensors Based on One Dimensional Nanostructured Metal-Oxides: A Review. *Sensors* **2012**, *12*, 7207–7258.
- (50) Yu, Y.; Hu, S.; Su, L.; Huang, L.; Liu, Y.; Jin, Z.; Purezky, A. A.; Geohegan, D. B.; Kim, K. W.; Zhang, Y.; et al. Equally Efficient Interlayer Exciton Relaxation and Improved Absorption in Epitaxial and Nonepitaxial MoS₂/WS₂ Heterostructures. *Nano Lett.* **2015**, 486.
- (51) Gurarslan, A.; Yu, Y.; Su, L.; Yu, Y.; Suarez, F.; Yao, S.; Zhu, Y.; Ozturk, M.; Zhang, Y.; Cao, L. Surface-Energy-Assisted Perfect Transfer of Centimeter-Scale Monolayer and Few-Layer MoS₂ Films onto Arbitrary Substrates. *ACS Nano* **2014**, *8*, 11522–11528.